Civil and Environmental Engineering
Vol. 0, Issue 0, DOI: 10.2478/cee-2026-0076

Seismic Behaviour of Long Links in Eccentrically Braced Frames Strengthened with Steel Plate and Diagonal Stiffener

Maiyozzi CHAIRI[1,3], Sabril HARIS[2*], Rendy THAMRIN[2], YURISMAN[4]

[1] Doctoral Student, Civil Engineering Department, Universitas Andalas, Padang, Indonesia

[2] Department of Civil Engineering, Universitas Andalas, Padang, Indonesia.

[3] Department of Civil Engineering, Universitas Putra Indonesia Yptk, Padang, Indonesia.

[4] Department of Civil Engineering, Politeknik Negeri Padang, Padang, Indonesia.

* corresponding author: sabril.haris@eng.unand.ac.id

Date of Submission: 29 October 2025
Revision Date: 01 January 2026
Date of Acceptance: 02 January 2026

Civil and Environmental Engineering
Journal of the Faculty of Civil Engineering | University of Žilina

Abstract

The structural damage observed in buildings highlights the crucial need for improved design quality in seismic-resistant construction systems, particularly for steel structures. This necessitates the development of earthquake-resistant structural systems that perform effectively both technically and architecturally. This study investigates the seismic behaviour of long links in Eccentrically Braced Frames (EBFs) strengthened using a hybrid method that combines flange thickening steel plate, and diagonal stiffeners. Five specimens were constructed and tested under cyclic lateral loading according to AISC-341-16 protocols. The specimens include one control link and four variations of flange and web strengthening, which were modified based on previous research. The research aims to propose novel strengthening methods that correlate the seismic performance of conventional structures with variations of the effective long link. Test specimens and experimental setups were designed considering boundary conditions and structural laboratory limitations. Results indicate that the specimens that were strengthened at both ends and mid-span with flange thickening and diagonal stiffeners attained the peak structural load capacity (27.48% increase) and stiffness (28.47% increase). However, its energy dissipation capacity was compromised by the implementation of stiffeners, which constrained plastic zone development. The specimen with only flange thickening demonstrated the highest ductility (1.54) and best energy efficiency (38.90%). Experimental results confirm that the hybrid strengthening technique effectively enhances cyclic performance in long-link EBFs, addressing both strength and ductility requirements in seismic-resistant structures.

Keywords

Long link; Eccentrically braced frames; Seismic behaviour; Steel Plate; Seismic Strengthening; Diagonal Stiffener.

1. Introduction

Earthquakes have fatal consequences for human lives and infrastructure. Therefore, building structures—particularly multi-story buildings—must incorporate seismic resilience through the use of high-quality materials and proper construction methods. SNI 254-2019 recommends a ductility-based approach, where specific structural components are intentionally designed to undergo controlled damage (plastic deformation) during major earthquakes, thereby preventing total collapse (SNI, 254 (2019)). Steel is one of the most effective materials for resisting seismic loads due to its exceptional

strength and ductility. The material offers significant construction advantages, including more straightforward implementation, more practical detailing and connections, and faster erection times. Structural systems must be designed with adequate strength to carry gravity loads and sufficient ductility to resist lateral excitations, thereby preserving stability and safety under various loading conditions (Gottem, et al., 2023).

There are three types of seismic-resistant steel structural systems commonly used: Moment Resisting Frames (MRF), Concentrically Braced Frames (CBF), and Eccentrically Braced Frames (EBF) (Chairi, Zaidir, Haris, & Yurisman, 2023). Eccentrically Braced Frames (EBF) are considered particularly effective for earthquake resistance due to their optimal combination of high ductility and stiffness (Ghobarah & Ramadan, 1990) (Binder, Gray, C, & O, 2017) (Yurisman, Army, Sari, & Chairi, 2021). The EBF system resists lateral loads by combining frame and truss actions. In other words, it can be viewed as a hybrid system between Moment Resisting Frames (MRF) and Concentrically Braced Frames (CBF). EBF provides high ductility similar to MRF while simultaneously offering elastic stiffness comparable to CBF (Daneshmand & Hashemi, 2012) (Yurisman, Sari, Murdiansyah, Chairi, & Khadavi, 2025). The behavioural differences between these three seismic-resistant steel structural systems are illustrated in Figure 1.

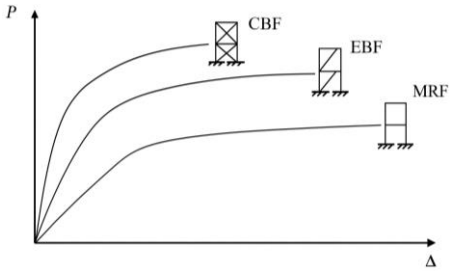

Figure 1: Differences in the behaviour of the three models of steel structural systems (Yurisman, Budiono, Moestopo, & Suarjana, 2010) (Daneshmand & Hashemi, 2012) (Yurisman, Sari, Murdiansyah, Chairi, & Khadavi, 2025)

The structural element called the Link acts as a structural 'fuse' in EBF systems, specifically designed to exhibit inelastic behaviour under extreme loading conditions. Links are categorised into short (shear-dominated), intermediate, and long (flexure-dominated) links (Bruneau, Uang, & Whittaker, 2011) (Engelhardt & Popov, 1992). Research indicates that long links demonstrate lower ductility and energy dissipation capacity compared to short links. However, from an architectural perspective, longer links provide greater spatial flexibility for openings like doors and windows (Malley, James, & Popov, 1984) (Hjelmstad, Keith, & Popov, 1984). Figure 2 illustrates an implemented EBF system featuring link elements as the designated yielding components (ANSI/AISC & 341-16, 2016) (Azad & Topkaya, 2017) (Yurisman, Sari, Murdiansyah, Chairi, & Khadavi, 2025). Figure 3 presents a 3D numerical model of a long link installation within an EBF frame.

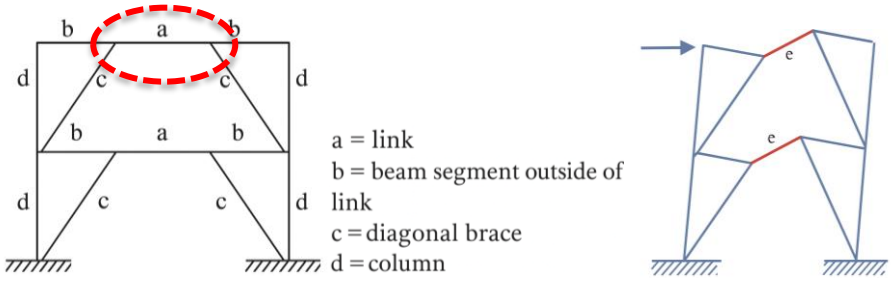

Figure 2: Configurations of Eccentrically Braced Frames and link yielding mechanism (ANSI/AISC & 341-16, 2016) (Yurisman, Sari, Murdiansyah, Chairi, & Khadavi, 2025) (Azad & Topkaya, 2017)

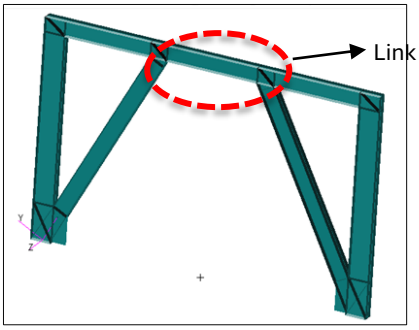

Figure 3: Long link in EBF Portal (Nastran, 2023) (Chairi, Zaidir, Haris, & Yurisman, 2023)

Eccentrically Braced Frames (EBFs) are widely recognized as an effective seismic force-resisting system due to their ability to dissipate energy through controlled yielding of link elements. Although extensive research has focused on short and intermediate links, the seismic behavior of long links remains relatively underexplored, particularly with respect to strengthening strategies that balance strength, stiffness, and ductility. In practice, long links are often strengthened to mitigate local buckling and excessive deformation; however, improperly configured or excessive strengthening may increase stiffness at the expense of ductility and energy dissipation, thereby undermining seismic performance. Moreover, current design provisions offer limited guidance on optimizing strengthening configurations for long links, especially concerning the combined use of flange thickening and diagonal stiffeners. Motivated by this gap, the present study experimentally investigates the seismic behavior of conventional and strengthened long EBF links in terms of strength, stiffness, ductility, and energy dissipation, and proposes strengthening strategies using flange steel plates and diagonal stiffeners to improve long-link performance toward that of more ductile short links. Recent studies have shown that external strengthening systems significantly enhance shear resistance and deformation capacity of structural members subjected to seismic-type loading, particularly after the initiation of diagonal cracking (Dewi, Thamrin, Haris, & Yastari, 2024).

2. EBF Link Behaviour and Failure Modes

From the 1970s through the 1980s, Eccentrically Braced Frames (EBF) emerged as the structural system of choice in high-seismicity regions (Malley, James, & Popov, 1984) (Roeder & Popov, Inelastic behaviour of eccentrically braced frames, 1977) (Roeder & Popov, Cyclic shear yielding of wide-flange beams, 1978) (Kasai & Popov, General behavior of WF steel shear link beams, 1986) (Kasai & Popov, A study of seismically resistant eccentrically braced frames, 1986) (Engelhardt & Popov, 1989). Research consistently demonstrated that short links outperformed intermediate and long links in terms of both strength and ductility under cyclic loading conditions (Roeder & Popov, Cyclic shear yielding of wide-flange beams, 1978) (Hjelmstad, Keith, & Popov, 1984). Early studies on long and intermediate links documented the gradual transition from shear-dominant to flexure-dominant behaviour (Engelhardt & Popov, 1989). The AISC provisions reflect these findings, with short links permitted higher rotation capacities (up to 0.08 radians) compared to long links (limited to 0.02 radians) (ANSI/AISC & 341-16, 2016).

Recent EBF research has identified multiple strengthening methods and variations applied to link components as single beams (sub-assemblies). In 2010 and more recently in 2025, Yurisman et al. conducted studies on short link performance using diagonal web stiffeners, comparing the behaviour of these strengthened shear links with conventional short links (Yurisman, Budiono, Moestopo, & Suarjana, 2010) (Yurisman, Sari, Murdiansyah, Chairi, & Khadavi, 2025). Various strengthening methods have been explored in other studies, including vertical stiffeners for short links (Dusicka, Itani, & Buckle, 2010), elastomeric web cores for long links (Stephens & Dusicka, 2014), haunched links with reduced mid-sections for intermediate/long links (Mansouri, 2021), stiffeners for short links in castellated steel beams (Mohebkhah, 2020), additional double stiffeners at long link ends (Musbar, Kusumastuti, & Setio, 2017), transverse stiffener variations for short links in stainless steel (Chacon, Vega, & Mirambell, 2019), residual stress investigations in link beam welds (Kurdi, Budiono, Moestopo, Kusumastuti, & Muslih, 2017), dual vertical link configurations (Rezaeian, Shayanfar, & Jelokhani, 2022), Shape

Memory Alloy (SMA) self-centering EBF systems with vertical links (Garmeh, Akbarpour, Adibramezani, Kashani, & Adibi, 2022). Most studies propose strengthening methods primarily for short links, with limited research on other types of links. Additionally, these investigations have employed various steel grades and cross-section profiles.

2.1. Link Element Characteristic

The use of long links in EBF systems significantly reduces inelastic deformation capacity (e > 2.6 Mp/Vp) where Mp is the plastic moment capacity and Vp is the plastic shear capacity. This aligns with fundamental experimental test results, which demonstrate that flexural mechanisms dominate link response. When the e-value exceeds 2.6 Mp/Vp (where the moment at the plastic hinge equals 1.2 Mp, the corresponding shear for such links becomes 0.92Vp). In the transition region where 1.6Mp/Vp < e < 2.6Mp/Vp, links experience simultaneous shear and flexural yielding (Engelhardt & Popov, 1992). For design purposes, EBF links are classified into three types, as illustrated in Figure 4: short links (shear-dominated), intermediate links, and long links (flexure-dominated).

The link rotation angle refers to the plastic rotation angle between the link and the surrounding frame members. Experimental studies demonstrate that the inelastic rotation capacity of links depends significantly on link length - shorter links exhibit greater rotation capacity (Kasai & Popov, A study of seismically resistant eccentrically braced frames, 1986). To achieve enhanced rotation capacity, intermediate links require closely spaced stiffeners. The permissible deformation capacity of links is specified in (ANSI/AISC & 341-16, 2016). Links are classified based on their yielding mechanism: shear links (short) yield dominated by shear forces, flexural links (long) yield dominated by bending moments, and intermediate links yield through combined shear and flexural action. The shear span represents the distance between the point of zero moment (inflection point) and the maximum moment location in the absence of intermediate loads. A balanced strength ratio occurs when both shear and flexural strains yield simultaneously. Figure 5 illustrates the behavioural mechanism of the EBF system links, demonstrating the concept of simple shear strain.

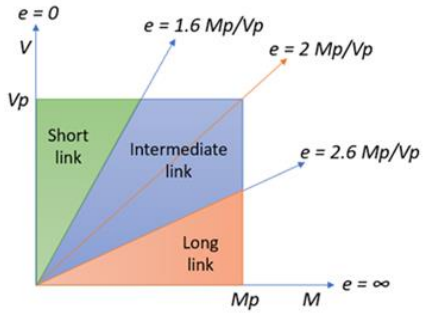

Figure 4: Link Classification, modified from (Bruneau, Uang, & Whittaker, 2011)

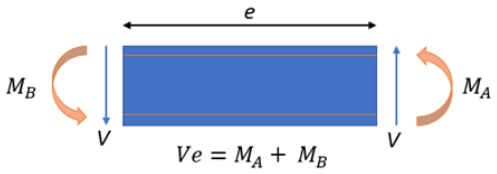

Figure 5: Deformation of link (free body diagram), modified from (Bruneau, Uang, & Whittaker, 2011)

A cantilever beam loaded at its free end represents the simplest form of shear strain, as demonstrated by the formula:

$$a = \frac{M}{V} \quad (1)$$

The equation gives the cantilever length under balanced strength conditions:

$$a_b = \frac{M_p}{V_p} \quad (2)$$

Where:

$$M_p = Z_x . F_y \quad (3)$$

$$V_p = 0.6. F_y. d. t_w \quad (4)$$

Where a = Shear span length of the cantilever beam, M = Applied moment on the beam vs M_p = plastic moment capacity of the link section and V = Applied shear force on the beam vs, V_p = plastic shear capacity of the link section, a_b = Balanced strength ratio, Z_x = plastic section modulus about x-axis, d = depth of W-shaped beam section, t_w = web thickness of steel section, F_y = steel material yield stress. In design criteria, the link is treated as a beam restrained at both ends, and the following equation determines the balanced condition link length (e_b):

$$e_b = 2. a_b = 2. \frac{M_p}{V_p} \quad (5)$$

2.2. Link Failure Mode

The performance of eccentrically braced frames (EBFs) is highly influenced by the behaviour of the link elements, which are subjected to significant inelastic deformations during seismic loading. Depending on their length, links can be classified into short links, intermediate links, and long links, each demonstrating different dominant failure mechanisms. For short links, the behaviour is primarily governed by inelastic shear deformation, with web buckling being the critical mode of failure. This instability arises from high shear demand concentrated on the web. The application of lateral stiffeners has been shown to mitigate this effect by restraining the web, thereby improving ductility and shear capacity (Bruneau, Uang, & Whittaker, 2011) (ANSI/AISC & 341-16, 2016) (Dusicka, Itani, & Buckle, 2010) (Yurisman, Budiono, Moestopo, & Suarjana, 2010).

Intermediate links exhibit a combination of shear and flexural deformation, resulting in a mixed failure mode. In these links, both shear web buckling and flange yielding or buckling can occur simultaneously. This dual mechanism makes their behaviour more complex compared to short or long links. Proper stiffening is therefore essential to control both shear- and flexure-related instabilities, ensuring that the link can achieve stable hysteretic behaviour under cyclic loading (Bruneau, Uang, & Whittaker, 2011) (Daneshmand & Hashemi, 2012).

For long links, the dominant response is flexural, with typical failure modes including flange fracture and flange buckling due to excessive flexural demands. Long links are also susceptible to lateral-torsional buckling, which can significantly reduce their load-carrying capacity and stability. The introduction of lateral stiffeners has proven effective in enhancing link stability and mitigating out-of-plane deformations (Bruneau, Uang, & Whittaker, 2011) (Engelhardt & Popov, 1989).

3. Experimental Study

The specimen uses WF 150×75×5×7 mm link beam sections, as shown in Figure 6. The selection of this profile accommodates laboratory constraints and testing frame limitations. Although relatively small compared to commonly used building profiles (WF 250 and larger), it remains representative for modelling EBF link behaviour. The WF 150 section is readily available in local markets, cost-effective, and satisfies geometric ratio requirements per AISC standards (ANSI/AISC & 341-16, 2016). All models employ stiffeners with identical thickness (t_s = 8 mm). The parametric study for these long-link specimens calculates the required link length as follows. The research adopts a link length ratio of e = 3.93 M_p/V_p, yielding a calculated link length of 960 mm."

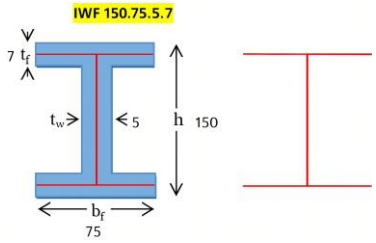

Figure 6: Steel profile used for specimens (modified of (Yurisman, Budiono, Moestopo, & Suarjana, 2010)

Tensile test data were obtained from the test results and mechanical properties. With the following material properties: Young's modulus (E) = 200,000 MPa, yield strength (Fy/Yp) = 343 MPa, Poisson's ratio (v) = 0.3. Elongation = 21%, and maximum tensile strength (Fu/Ts) = 477 MPa. Modified long-link specimens based on performance evaluations from prior studies. The core modification concept aims to achieve short-link performance characteristics in the designed long links. Detailed configurations for the modified test specimen dimensions are provided in Table 1. The 960 mm link length was determined from the long link ratio for the 150×75×5×7 mm profile, yielding e = 3.93 M_p/V_p (e > 2.6 M_p/V_p), which supports the rationale behind the specimen design. The LL-0 specimen, as the baseline design for long links, complies with AISC 341-16. LL-1 (thickened Flange + vertical stiffeners at L/3), based on prior research demonstrating that long links typically yield in flange regions near the ends, under flexural dominance design complies with AISC 341-16 provisions for flexure-dominated links. LL-2 (thickened flange + vertical stiffeners at L/3 + mid-web diagonal stiffener) adapted from short link strengthening strategies (e ≤ 1.6Mp/Vp) investigates: Stress distribution in longitudinally stiffened long links and combined flange-web strengthening effectiveness. LL-3 (thickened flange + vertical stiffeners at L/3 + end-web diagonal stiffeners) implements end-stiffening solutions from previous studies, showing a 20-25% stiffness improvement and delayed web buckling initiation. LL-4 (thickened flange + vertical stiffeners at L/3 + combined mid- and end-web diagonal stiffeners), hybrid solution targeting: Optimal stress redistribution and enhanced cyclic performance beyond AISC 341 requirements.

Table 1: Test specimen specification

ID	Modified Links		
	Flange end thickening (1/3 L) [mm]	Midspan diagonal stiffener (1/3 L) [mm]	End diagonal stiffener plate (1/3 L) [mm]
LL-0	-	-	-
LL-1	8	-	-
LL-2	8	8	-
LL-3	8	-	8
LL-4	8	8	8

Experimental testing was conducted on a control specimen model designed by (ANSI/AISC & 341-16, 2016) and four strengthened specimen models. The test specimens were constructed with predetermined dimensions for experimental evaluation. The details and constructed dimensions of the test specimens are illustrated in Figures 7 and 8. The red-colored part represents the additional link that was modified as strengthening.

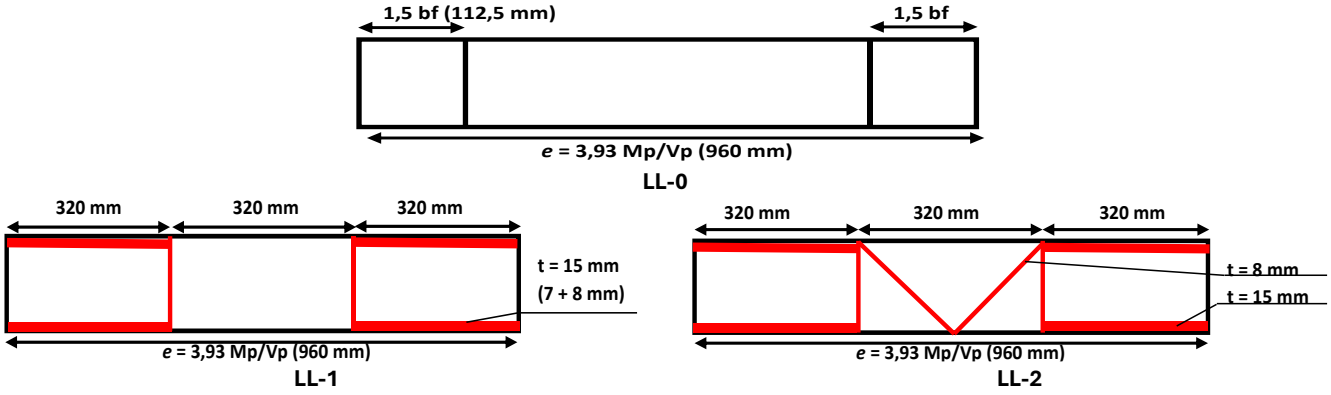

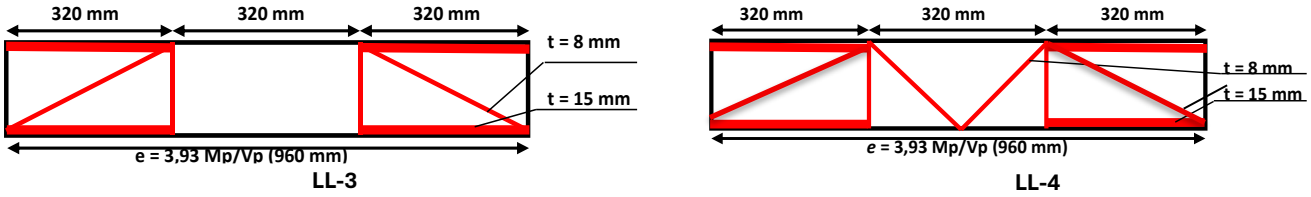

Figure 7: Test specimen details

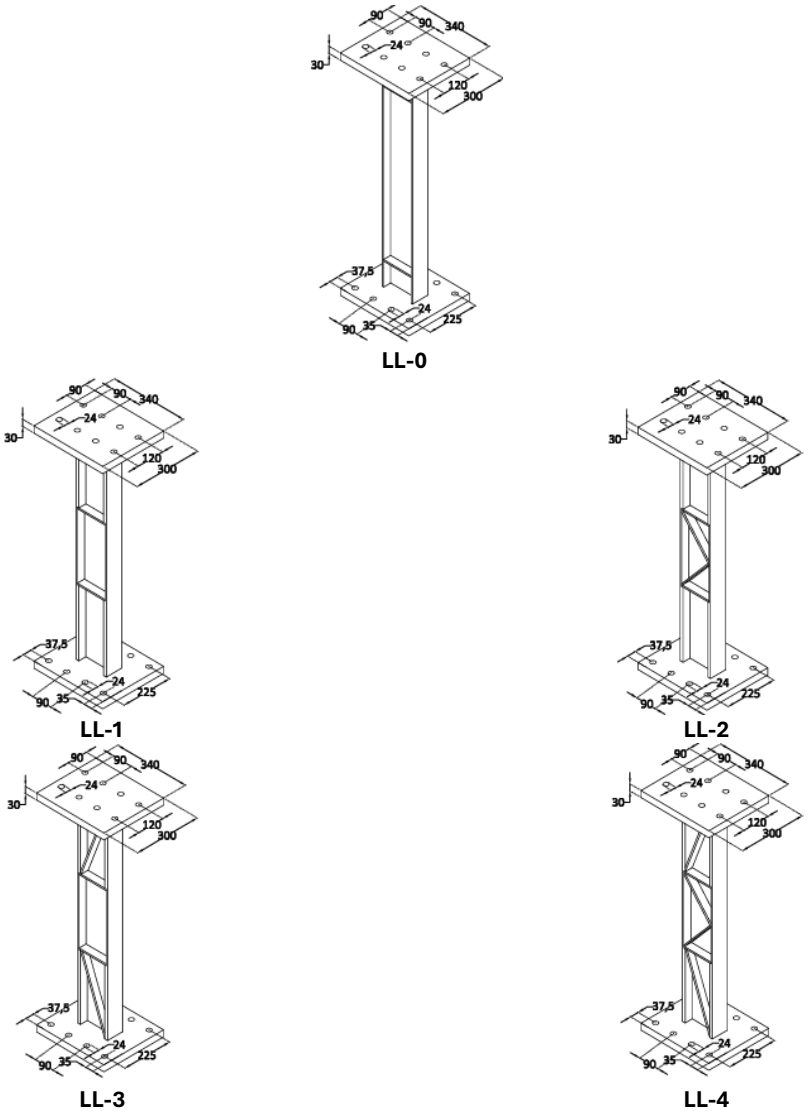

Figure 8: The constructed dimensions for testing specimens with an endplate (Isometri)

The loading protocol follows (ANSI/AISC & 341-16, 2016) Standards. The loading sequence for test specimens was designed according to the total link rotation angle. The loading protocol adheres to established guidelines for link beams, as illustrated in Figure 9. The load history for testing consisted of two cycles for each loading increment, as shown in Figure 10.

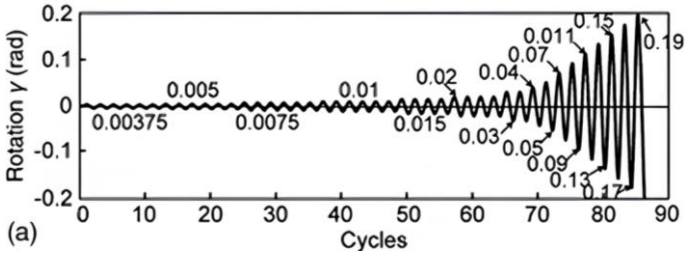

Figure 9: Reference loading protocol for link beams (ANSI/AISC & 341-16, 2016)

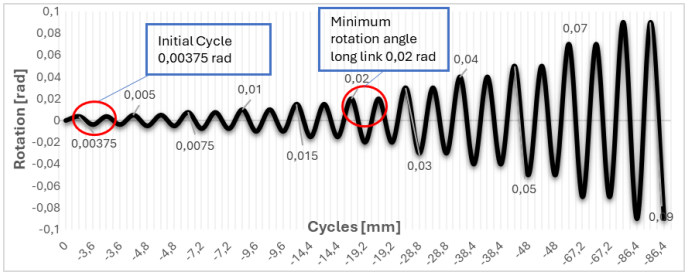

Figure 10: Experimental loading protocol, adopted from (ANSI/AISC & 341-16, 2016)

The proposed study will utilize long link specimens in an EBF system to experimentally analyze their seismic performance (strength, stiffness, ductility, and energy dissipation), and then develop a strengthening method that evaluates the relationship between the seismic performance of control length links and the variation in effective link length. Length variation will be implemented by thickening the steel plates at the flanges by 1/3L at both ends. Diagonal stiffeners will then be added at the mid-span and web end locations of the specimens, with assembly completed using end plates.

Both specimen preparation and test setup were adapted to accommodate the existing equipment limitations. The tests were performed under cyclic loading conditions, with the experimental setup configuration shown in Figure 11. Following testing, the experimental data were processed and analysed to evaluate the results.

Figure 11: Initial test setup planning

The boundary conditions in the experimental test setup consist of the following configurations: Both ends of the steel profile (end plates) are fixed—the lower side is fixed to the base plates. In contrast, the upper side is restrained by supporting H-beams (300 × 300 × 10 × 15 mm). The left and right support beams (H-beams 200 × 200 × 8 × 12 mm) are modelled as pinned connections. The lower section of the steel profile (test specimen) is fully fixed, while the upper section is permitted to translate in only one direction (horizontally, along the x-axis). To prevent out-of-plane displacements, all four sides of the upper support beams (which transfer the applied load) are laterally restrained using sling mechanisms.

The boundary conditions were calibrated against the numerical model using MSc Patran/Nastran 2023 software. The long link was discretized into quadrilateral shell elements with fully fixed moment constraints applied at both ends. The loading nodes were constrained to permit translation exclusively along the y-axis, simulating a restrained yet deformable boundary condition characteristic of eccentrically braced frame connections. This complex force redistribution mechanism in long links was effectively captured by the modeling technique. Figure 12 is included to illustrate the applied boundary conditions, loading direction, and finite element discretization adopted in the numerical model, which were used to support and interpret the experimentally observed deformation and failure mechanisms (Chairi, Zaidir, Haris, & Yurisman, 2023).

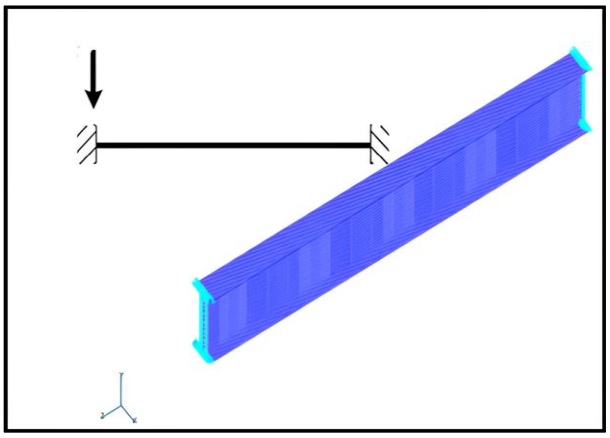

Figure 12: Finite Element Modelling for Long Link (Chairi, Zaidir, Haris, & Yurisman, 2023)

4. Results and Discussion

The Results and discussion section covers the performance of the tested long links, including both control long links and modified long links. The analysis focuses on seismic parameters, including strength, stiffness, ductility, and energy dissipation.

4.1. Initial Yielding and Peak Load

Initial yielding in the test specimens was marked by localized paint flaking, with varying patterns observed. Generally, all specimens yielded by the 6th loading cycle. However, the ultimate load and failure conditions occurred at different cycles for each specimen. Control specimen LL-0 exhibited paint flaking during Cycle 6A at the flange near the stiffener (1.5 bf distance) and the end-plate flange. Specimen LL-1 showed flaking during Cycle 6B at the stiffener-adjacent flange (1/3 L distance), followed by web flaking. Specimens LL-2, LL-3, and LL-4 primarily experienced paint flaking at the flange ends and web. The experimental results are illustrated in Figure 13 and Table 2. The experimental backbone curves are presented in Figure 14. For both positive and adverse loading conditions, Cycle 7B serves as the comparable state, with an average displacement of 28.8 mm across all tests. Specimen LL-4, followed by LL-1, achieved the highest load capacity. These results demonstrate consistency, since the synergistic effect of increased flange thickness and strengthened diagonal stiffeners significantly enhances the specimen's resistance to applied loads. This behaviour is consistent with previous experimental findings by (Engelhardt & Popov, 1989) and (Daneshmand & Hashemi, 2012), who reported that flexure-

dominated long links benefit primarily from flange strengthening, while excessive web stiffening tends to shift yielding away from the intended plastic hinge regions.

Figure 13(a), Yield initiation: paint flaking observed at the stiffener-proximate flange (specimen LL-0, 5A Cycle).

Figure 13(b), Ultimate condition: flange buckling observed at both top and bottom flange regions (specimen LL-0, 10A Cycle).

Figure 13(c), Failure condition: tensile fracture at the bottom flange (specimen LL-0, 10B Cycle).

Figure 13(d), Yield condition: paint flaking observed on the flange section (specimen LL-1, 6B Cycle).

Figure 13(e), Ultimate condition: extensive paint flaking observed on both web and flange sections (specimen LL-1, 8A Cycle).

Figure 13(f), Failure condition: fracture at weld-adjacent flange region (specimen LL-1, 8B Cycle).

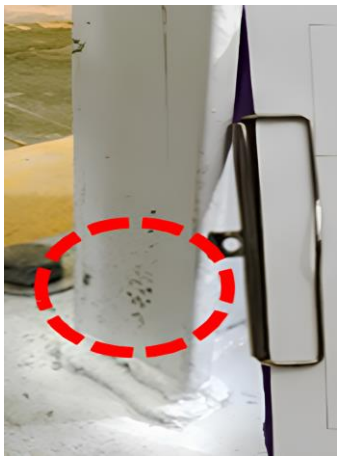

Figure 13(g), Yield condition: paint flaking observed at stiffener-proximate flange (specimen LL-2, 6B Cycle).

Figure 13(h), Ultimate condition: extensive paint flaking observed at the end-region of the web (specimen LL-2, 8B Cycle).

Figure 13(i), Failure condition: fracture at the upper weld region (specimen LL-2, 9B Cycle).

Figure 13(j), Yield condition: paint flaking observed at the stiffener-adjacent flange with minor flaking in the web region (specimen LL-3, 6B Cycle).

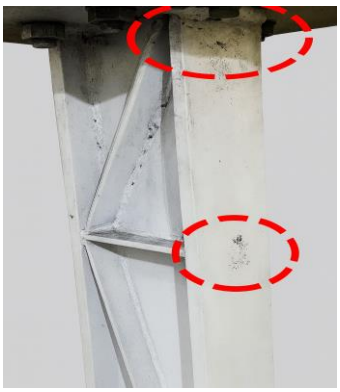

Figure 13(k), Ultimate condition: paint flaking observed at both the flange end and stiffener-proximate regions (specimen LL-3, 8A Cycle).

Figure 13(l), Failure condition: fracture at weld location (specimen LL-3, 8A Cycle).

Figure 13(m), Yield condition: paint flaking observed on the flange (specimen LL-4, 6B Cycle).

Figure 13(n), Ultimate condition: progressive paint flaking at the flange tip (specimen LL-4, 7A Cycle).

Figure 13(o), Failure condition: fracture at the top weld location (specimen LL-4, 8A Cycle).

Figure 13: Visual inspection of experimental outcomes

Table 2: Test specimen condition overview

No	ID	Yield			7B Cycle (0.03 rad)			Ultimate			Failure		
		Cycle	Displacement [mm]	P [kN]	Cycle	Displacement [mm]	P [kN]	Cycle	Displacement [mm]	P [kN]	Cycle	Displacement [mm]	P [kN]
1	LL-0	6A	19.26	72.36	7B	29.04	85.66	10A	67.20	107.80	10B	67.20	60.68
2	LL-1	6B	19.30	83.24	7B	28.89	106.84	8B	38.40	116.00	8B	34.86	106.02
3	LL-2	6B	19.41	79.50	7B	28.83	102.54	9A	48.00	124.30	9B	48.00	69.60
4	LL-3	6B	19.32	78.34	7B	28.92	100.60	7B	28.80	100.60	8A	38.40	67.72
5	LL-4	6B	19.17	84.04	7B	28.80	109.20	7B	28.80	109.20	8A	38.30	64.80

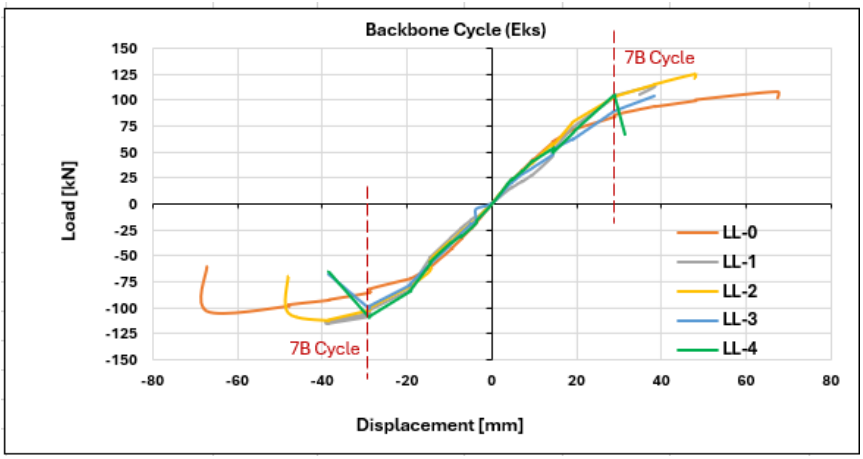

Figure 14: Experimental test backbone curve

4.2. Strength

The strength values were obtained from the peak load capacity recorded in each loading sequence from Cycle 1A to 7 B. The strength capacity at Cycle 7B (0.03 rad) serves as the comparable condition for all specimens, as it exceeds the minimum rotation requirement of 0.02 rad for long links. The improvements in the modified specimens' strength capacity relative to the control specimen are presented in Table 3. Key observations at Cycle 7B: LL-4 showed the highest strength increase at 27.48% LL-1, followed closely by 24.73% improvement. LL-2 and LL-3 demonstrated increases of 19.71% and 17.44%, respectively. The strength capacity progression for all specimens is graphically presented in Figure 15. These results indicate that the combined flange thickening with steel plate and diagonal stiffener strengthening significantly enhances the specimen's load-bearing capacity.

Table 3: Specimens Strength Capacity (Control and Modification)

Specimens Modifications	Yield				7B Cycle (0.03 rad)			
	Load [kN]	Specimens Control	Load [kN]	Enhancement	Load [kN]	Specimens Control	Load [kN]	Enhancement
LL-1	83.24	LL-0	72.36	15.04%	106.84	LL-0	85.66	24.73%
LL-2	79.50	LL-0	72.36	9.87%	102.54	LL-0	85.66	19.71%
LL-3	78.34	LL-0	72.36	8.26%	100.60	LL-0	85.66	17.44%
LL-4	84.04	LL-0	72.36	16.14%	109.20	LL-0	85.66	27.48%

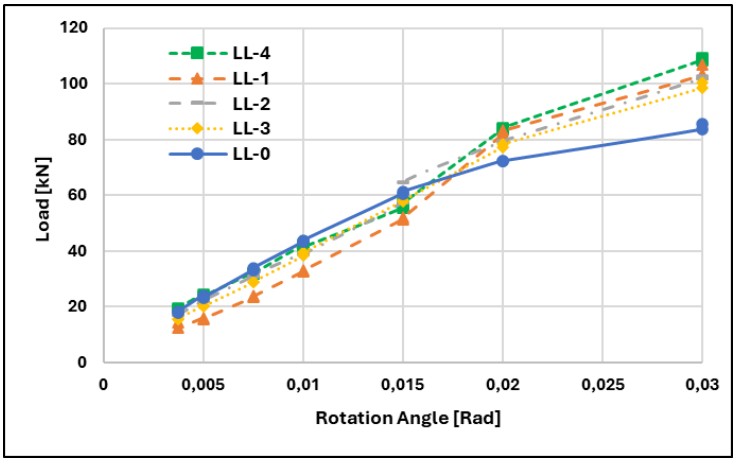

Figure 15: Experimental test backbone curve

The overall analysis reveals that all test specimens exhibit a significant increase in load capacity compared to LL-0 (AISC 341-16). The highest improvement is achieved by LL-4, followed by LL-1, LL-2, and LL-3. This indicates that the combination of flange thickening and web stiffeners (vertical and diagonal) significantly enhances resistance to cyclic (seismic) loading. Each specimen demonstrates distinct behaviour, reflecting the relationship between strength and its specific modification configuration. Performance breakdown by Specimen. LL-1 (thickened flange + vertical stiffeners at L/3) achieves the second-highest strength increase (24.73%), despite lacking diagonal stiffeners; flange thickening alone contributes substantially, resulting in high efficiency with minimal modifications. LL-2 (thickened flange + vertical stiffeners at L/3 + mid-web diagonal stiffener) shows a significant strength improvement (19.71%), demonstrates balanced deformation and strength, maintains stability under rotation and cyclic seismic loads, and provides enhanced resistance to shear deformation in the mid-web region. LL-3 (thickened flange + vertical stiffeners at L/3 + end-web diagonal stiffeners) exhibits a more minor strength increase (17.44%) compared to LL-2, diagonal stiffeners at the ends offer limited global resistance to internal forces, leading to stress concentration in the mid-web and suboptimal performance. LL-4 (thickened flange + vertical stiffeners at L/3 + Combined Mid- and End-Web Diagonal Stiffeners) delivers the highest strength increase (27.48%) but tends to be excessively stiff; earlier hysteresis curve analysis shows rapid narrowing, indicating brittle response tendencies.

The experimental results demonstrate that flange thickening contributes to an increase in both yield and ultimate strength, indicating its effectiveness in enhancing the load-carrying capacity of long EBF links. The incorporation of vertical stiffeners at approximately one-third of the link length was observed to mitigate local buckling and promote a more uniform force distribution along the link. Among the investigated configurations, the mid-web diagonal stiffener arrangement (LL-2) exhibited a comparatively stable and balanced seismic response, characterized by a favorable combination of strength and deformation capacity. In contrast, specimens employing combined diagonal stiffeners (LL-4) achieved the highest strength enhancement but exhibited a reduction in plastic deformation capacity, suggesting that excessive stiffening may adversely affect ductility. These observations highlight the inherent trade-off between strength enhancement and ductility preservation in strengthened long-link EBF systems. Similar strength enhancement trends have been reported by (Musbar, Kusumastuti, & Setio, 2017) and (Mansouri, 2021), where additional stiffening increased peak load capacity but also introduced higher stress concentration and reduced deformation flexibility in long or intermediate links.

4.3. Stiffness

Stiffness is defined as the ratio of applied force to resulting deformation. The experimental study revealed that specimens LL-4 and LL-1 exhibited higher stiffness values at both initial yielding and peak load compared to other specimens. During yield initiation and Cycle 7B, LL-4 (4.38 and 3.79) and LL-1 (4.31 and 3.70) demonstrated the highest stiffness. This enhanced performance is attributed to the 1/3L flange thickness extension and the 1/3L inward relocation of stiffeners, which collectively improve stiffness performance over control specimens and other test variants. The stiffness values and associated degradation curves are documented in Table 4 and illustrated in Figure 16.

Table 4: Test specimen stiffness coefficient

ID	Condition	Displacement [mm]	Rotation Angle [rad]	Load [kN]	Stiffness [N/m]
LL-0	Initial yielding	19.26	0.02	72.36	3.76
	Cycle 7B	29.04	0.03	85.66	2.95
LL-1	Initial yielding	19.30	0.02	83.20	4.31
	Cycle 7B	28.89	0.03	107.00	3.70
LL-2	Initial yielding	19.41	0.02	79.30	4.01
	Cycle 7B	28.83	0.03	102.00	3.56
LL-3	Initial yielding	19.32	0.02	77.30	4.05
	Cycle 7B	28.92	0.03	101.00	3.48
LL-4	Initial yielding	19.17	0.02	83.50	4.38
	Cycle 7B	28.80	0.03	109.00	3.79

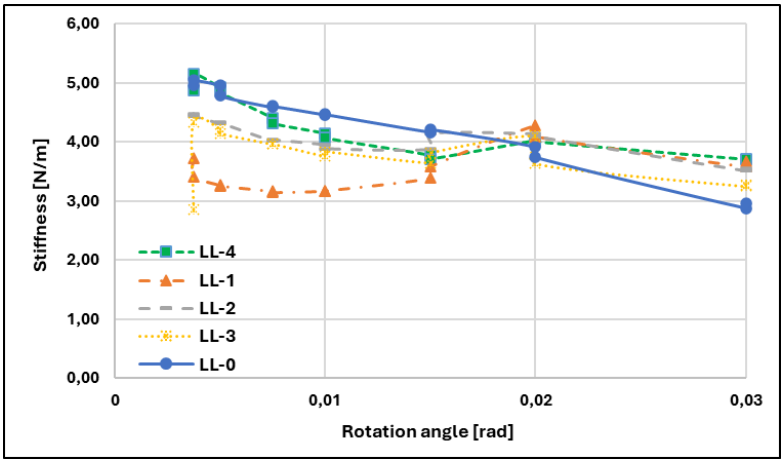

Figure 16: Experimental specimen stiffness curve

The stiffness curves of all test specimens exhibit a decreasing stiffness trend as the rotation angle increases. This is a typical behaviour in structural systems subjected to cyclic loading due to seismic forces, where stiffness degradation occurs as a result of accumulated plastic damage and micro-cracking in the material. Stiffness degradation is a critical indicator in assessing the cyclic resilience of a structural element. Elements with high initial stiffness but slow degradation are more effective in maintaining lateral stability and preventing premature instability. Specimens LL-1 and LL-2 exhibit the highest initial stiffness values, at 4.31 N/m and 4.01 N/m, respectively, highlighting the effective contribution of the thickened end-flange (1/3 L) in enhancing initial flexural stiffness. Meanwhile, LL-3 and LL-4 exhibit slightly higher stiffness than the control specimen, LL-0, at 4.05 N/m and 4.38 N/m, respectively, indicating the positive influence of diagonal stiffeners. LL-0 (AISC 341-16) records the lowest baseline stiffness at 3.76 N/m. For final stiffness (Cycle 7B), LL-4 and LL-1 exhibit the highest retained stiffness: 3.79 N/m and 3.70 N/m, followed by LL-2 (3.56 N/m) and LL-3 (3.48 N/m). In contrast, LL-0 suffers a significant drop to 2.95 N/m, reflecting severe stiffness degradation due to the absence of stiffening elements. LL-0 (AISC 341-16) shows a sharp and consistent decline in stiffness. At the same time, LL-1 (thickened flange + vertical stiffeners at L/3) displays stagnant and low performance throughout the cycles, suggesting that vertical stiffeners at L/3 contribute minimally to resistance under large rotational deformations. LL-2, LL-3, and LL-4 demonstrate better stiffness retention until the final cycles, with LL-2 showing the smallest decline and the flattest curve after a rotation of>0.02 rad (the lowest degradation value). Preliminary Analysis for Seismic Resilience (Stiffness-Based). Among the modified specimens, LL-2 proves to be the most effective in resisting stiffness degradation under cyclic seismic loading. The combination of thickened end-flanges (improving flexural capacity) and mid-web diagonal stiffeners (enhancing shear stiffness) creates a positive synergy, maintaining structural integrity without inducing internal force conflicts. This is evidenced by its lowest stiffness degradation (0.45) and high retained stiffness at large rotations. For comparison, LL-3 and LL-4 also perform well but with higher complexity (double stiffeners) and slightly lower structural efficiency (less economical) than LL-2.

4.4. Ductility (μ)

The optimal ductility performance values are presented in Table 5, evaluated at both initial yield displacement and peak load displacement (measured at first yield and Cycle 7B). Although the differences were not statistically significant, specimen LL-1 demonstrated superior ductility with a value of 1.54, outperforming the other four test specimens, including the control specimen (ductility = 1.51). The remaining specimens were ranked as follows: LL-4 (1.50), LL-3 (1.50), and LL-2 (1.49). This indicates LL-1's enhanced ability to undergo plastic deformation before failure. Visual observations confirmed that the 1/3L flange thickness extension at both ends effectively reduced failure risks. The ductility progression is graphically shown in Figure 17.

Table 5: Experimental ductility ratio of test specimen

ID	Condition	Displacement [mm]	Rotation Angle [rad]	Load [kN]	dy [mm]	du [mm]	μ	μ Average
LL-0 (+)	Yield	19.22	0.02	71.58	19.22	29.01	1.51	1.51
	7B Cycle	29.01	0.03	85.50				
LL-0 (-)	Yield	-19.26	0.02	-72.36	-19.26	-29.04	1.51	
	7B Cycle	-29.04	0.03	-85.66				
LL-1 (+)	Yield	16.68	0.02	74.86	16.68	26.53	1.59	1.55
	7B Cycle	26.53	0.03	104.58				
LL-1 (-)	Yield	-19.30	0.02	-83.24	-19.3	-28.89	1.50	
	7B Cycle	-28.89	0.03	-106.84				
LL-2 (+)	Yield	19.26	0.02	78.52	19.26	28.83	1.50	1.50
	7B Cycle	28.83	0.03	102.54				
LL-2 (-)	Yield	-19.41	0.02	-79.50	-19.41	-28.86	1.49	
	7B Cycle	-28.86	0.03	-102.30				
LL-3 (+)	Yield	19.26	0.02	62.02	19.26	28.86	1.50	1.50
	7B Cycle	28.86	0.03	88.70				
LL-3 (-)	Yield	-19.32	0.02	-78.34	-19.32	-28.92	1.50	
	7B Cycle	-28.92	0.03	-100.60				
LL-4 (+)	Yield	19.30	0.02	71.16	19.30	28.83	1.49	1.50
	7B Cycle	28.83	0.03	105.40				
LL-4 (-)	Yield	-19.17	0.02	-84.04	-19.17	-28.8	1.50	
	7B Cycle	-28.80	0.03	-109.20				

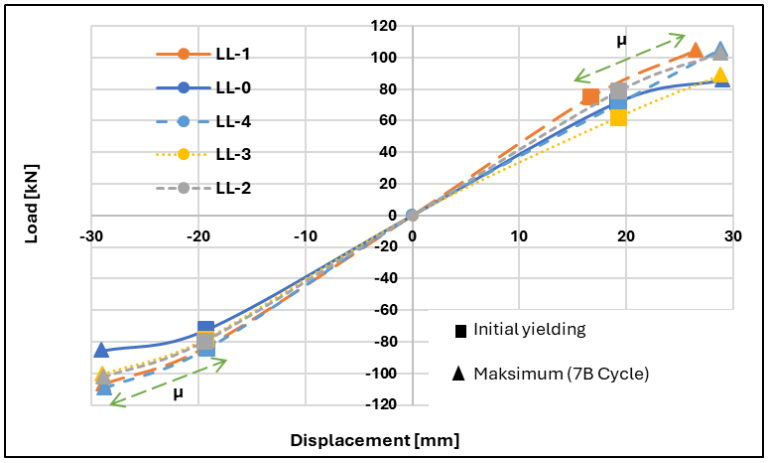

Figure 17: Experimental specimen ductility curve

Ductility Analysis Summary (Up to Cycle 7B). All test specimens demonstrated remarkably similar and consistent ductility values, ranging from 1.50 to 1.55. LL-1 exhibited the highest ductility (μ = 1.55), indicating superior plastic deformation capacity before instability or collapse. Interestingly, the control specimen LL-0 showed comparable or slightly higher ductility than some strengthened specimens (LL-2, LL-3, LL-4), suggesting that structural strengthening did not significantly enhance ductility and may occasionally slightly restrict plastic deformation. LL-1 Performance achieved peak ductility (μ = 1.55), flange thickening and vertical stiffeners at L/3 enabled greater post-yield deformation, exhibited minor load-direction asymmetry (±) within acceptable tolerance limits. LL-0 (Control) comparison matched or exceeded the ductility of LL-2, LL-3, and LL-4, confirming the baseline system's inherent plastic deformability; strengthening did not substantially improve ductility. The strengthening effects in LL-2, LL-3, and LL-4 stiffeners primarily enhanced stiffness and strength, rather than ductility. LL-4's strengthening slightly constrained pre-peak plastic deformation, resulting in marginally lower μ than LL-0. Among the tested specimens, the LL-1 configuration exhibited comparatively higher ductility, suggesting

that the combined flexural strengthening and vertical stiffeners contributed to a more stable plastic deformation mechanism without triggering premature instability. In contrast, specimens employing single-element strengthening strategies, such as isolated flange or web stiffeners (LL-2 to LL-4), did not demonstrate a noticeable improvement in ductility and, in some cases, showed a slight reduction in deformation capacity. This behavior may be attributed to localized stiffness concentration that constrained plastic rotation development. Overall, the results highlight that both the type and location of strengthening measures play an important role in influencing ductility performance; however, within the scope of the present study, these effects remained moderate. Comparable ductility levels for strengthened and unstrengthened long links have also been reported by (Engelhardt & Popov, 1992) confirming that ductility improvement in flexure-dominated links is more difficult to achieve through stiffening alone.

4.5. Energy Dissipation

The hysteretic curves presented in Figure 18 demonstrate varying energy dissipation capacities across all test specimens, showing the cumulative energy dissipation values from experimental testing. In long link EBFs, cumulative energy dissipation is defined as the area enclosed by the hysteresis loops from both loading cycles. A larger area reflects enhanced inelastic deformation capacity and improved seismic energy absorption. This variation stems from differences in the maximum achieved loading cycles for each specimen and Distinct failure modes (either within the link element itself or at the weld-to-endplate connection). Notably, pinching behaviour was observed in specimens LL-2 and LL-3, likely induced by local buckling. All specimens attained the target rotation angle of 0.02 rad for long links. For experimental comparison, the 0.03 rad cycle performance (Cycle 7B at a 28.8 mm displacement) was analysed, with energy dissipation comparisons presented in Table 6.

The control specimen LL-0 exhibited both the largest individual cycle area and total cumulative area up to Cycle 7B, indicating superior energy dissipation capacity under cyclic loading compared to the four modified specimens. LL-1 (flange-thickened) achieved the second-best energy dissipation performance, demonstrating the highest proportional energy absorption (38.9%) during Cycle 7B relative to total cumulative energy. The control specimen displayed the highest energy dissipation, attributed to pinching effects and excessive stiffness in strengthened specimens caused by buckling. The Cycle 7B hysteresis area values (kN·mm) in descending order are LL-0 2450.61 kN·mm, LL-1 1980.50 kN·mm, LL-2 1308.70 kN·mm, LL-3 1301.99 kN·mm, LL-4 1193.67 kN·mm.

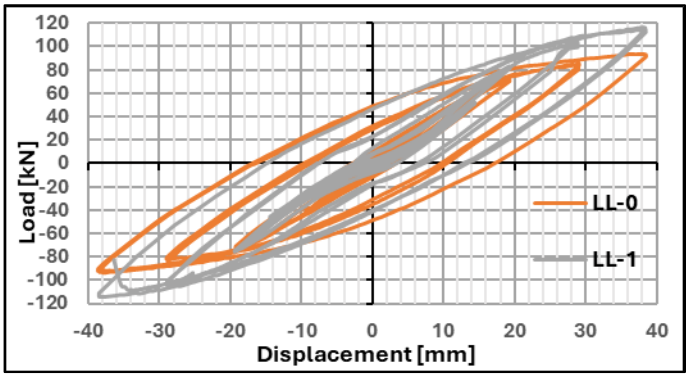

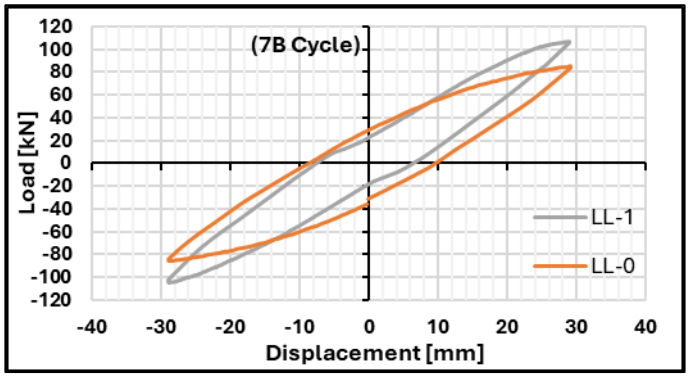

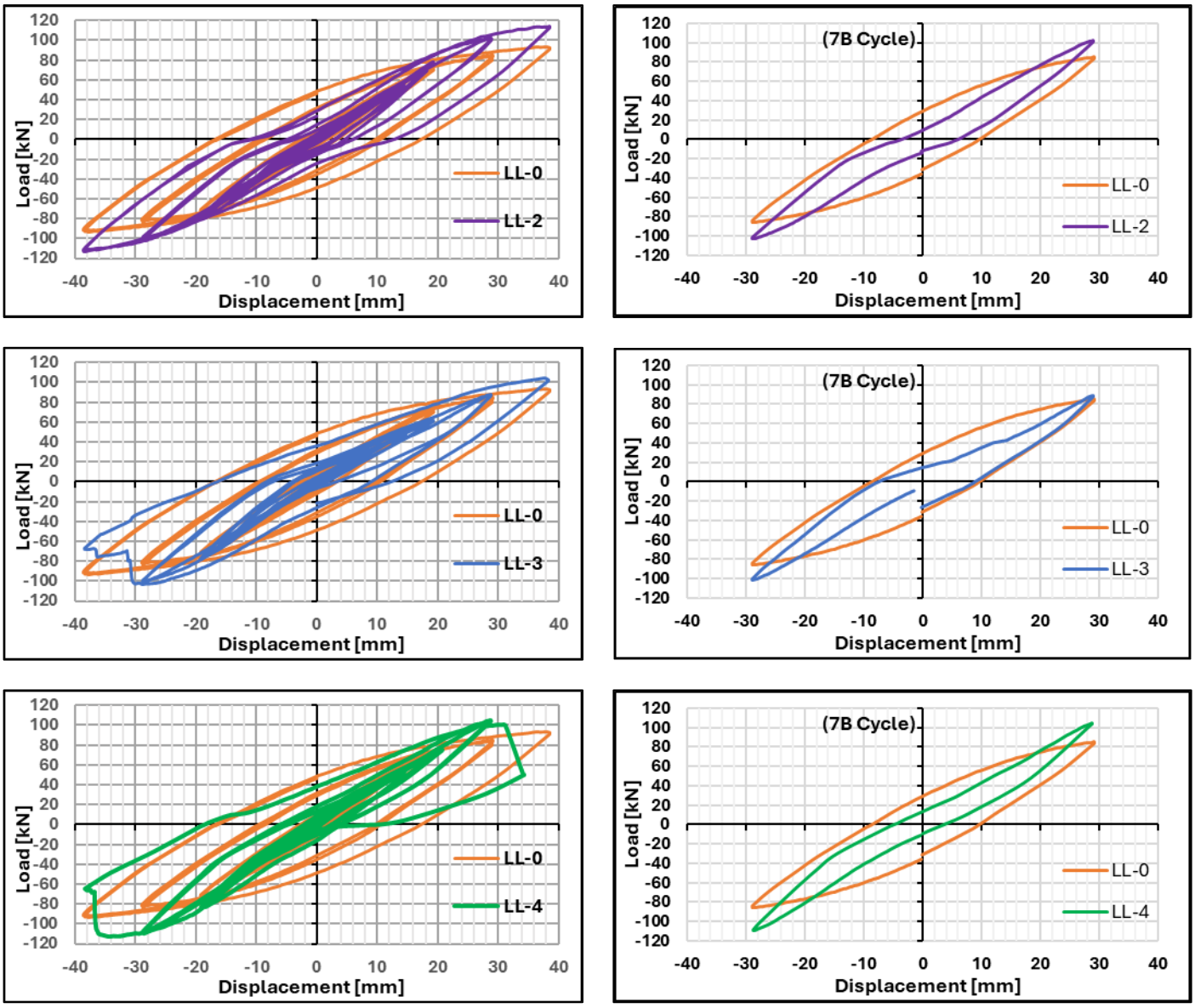

Figure 18: Experimental hysteretic loop and energy dissipation capacity at loading Cycle 7B

Table 6: Specimen energy dissipation based on hysteresis loop area

ID	Cycle Area 7B [kN · m]	Cumulative Dissipated Energy [kN · m]	Ratio (Cycle Area 7B/Cumulative Dissipated Energy)
LL-0	2.45	6.55	0.37
LL-1	1.98	5.08	0.39
LL-2	1.31	4.45	0.29
LL-3	1.30	4.34	0.30
LL-4	1.19	4.50	0.27

The control specimen LL-0 (AISC 341-16) exhibited the largest hysteresis loop area (2.45 kN·m at cycle 7B), demonstrating complete and stable hysteresis curves that indicate excellent plastic behaviour and high energy dissipation capacity. However, without additional strengthening, it may experience earlier collapse under extreme conditions. LL-1 (Flange Thickness + Vertical Stiffeners at L/3) slightly reduced hysteresis area (1.98 kN·m), achieved the highest energy dissipation ratio (0.39), maintained wide, stable hysteresis curves, demonstrated improved energy dissipation efficiency per cycle (7B), and modified preserved ductile behaviour without significant compromise. LL-2 (LL-1 + Mid-Web Diagonal

Stiffener) exhibits a substantial reduction in hysteresis area (1.31 kN·m) and energy ratio (0.29), with noticeably narrower hysteresis loops. It also shows increased stiffness but reduced plastic deformation capacity. The mid-web diagonal stiffener restricts local plastic rotation, limiting energy dissipation mechanisms. LL-3 (LL-1 + End-Web Diagonal Stiffeners) is nearly identical to LL-2 in both numerical values and hysteresis shape. End stiffeners constrain bending deformation, and performance is still superior to that of fully-stiffened LL-4, creating highly localised deformation zones. LL-4 (LL-1 + Combined Mid- and End-Web Diagonal Stiffeners) exhibits the most negligible energy dissipation (1.19 kN·m) and the lowest ratio (0.27), with the narrowest and sharpest hysteresis loops. Excessive stiffness led to significant energy dissipation loss, and overlapping stiffener interactions proved counterproductive. The primary analysis revealed that several modified specimens (LL-2, LL-3, LL-4) tended to reduce and limit energy dissipation. This is attributed to increased stiffness that constrains plastic zone development, coupled with excessive reinforcement—particularly diagonal stiffeners—which diminishes both ductility and energy dissipation capacity. In contrast, specimen LL-1 demonstrated the most efficient energy dissipation performance among modified variants, although it did not have the highest absolute value. The control specimen (LL-0) demonstrated that while unstrengthened sections have excellent energy dissipation, they may require strengthening to prevent premature collapse. Similar reductions in energy dissipation due to excessive stiffening were observed by (Stephens & Dusicka, 2014), and (Mohebkhah, 2020), where constrained plastic rotation led to narrower hysteresis loops despite increased strength. Another observation is that in reinforced concrete elements, excessive local reinforcement can increase stiffness and strength while negatively impacting ductility and energy dissipation capacity due to inhibited plastic deformation zones (Maulana, et al., 2025).

5. Conclusion

Five long joint specimens were tested and reported in this study. The behaviour of the proposed strengthening methods for the seismic performance of long joints was analysed, and effective strengthening techniques were identified. The main conclusions are as follows:

1) Addition of web diagonal stiffeners (LL-4) and flange thickening (applied at 1/3L on both ends) in LL-1 significantly improved the load capacity. However, specimens with only single web diagonal stiffeners (LL-2/LL-3) demonstrated lower effectiveness compared to LL-1.

2) Fractures occurred at the weld of the end plate in 3 of 5 specimens. However, the failure of the end-plate specimen could attain the target rotation, i.e. 0,02 radian

3) In this research, LL-1 is proposed as the most balanced and efficient modification, demonstrating: Reasonable strength and stiffness enhancement, highest ductility among all specimens, optimal energy dissipation ratio without excessive stiffness, most ductile seismic performance, and practical efficiency for real-world earthquake-resistant structures.

4) The combination of vertical stiffeners and L/3 flange strengthening provides excellent: Plastic deformation capacity, energy absorption, and structural stability. Selective diagonal stiffeners may be carefully considered for performance enhancement, provided they do not compromise ductility.

5) From a practical design perspective, the results suggest that strengthening strategies for long EBF links should prioritize balanced stiffness enhancement rather than maximum strength. Moderate and well-integrated strengthening layouts can improve seismic resilience while preserving the ductile behavior essential for energy dissipation.

6) The study is limited by the number of tested specimens, with only one specimen per strengthening configuration. Future research should include a larger experimental database, numerical analysis, detailed investigation of welded end-plate failure mechanisms, and full-scale testing of EBF subassemblies to capture global system interactions. Further exploration of alternative materials and combined strengthening techniques may also contribute to optimizing long-link EBF design in seismic regions.

Acknowledgements

The authors would like to acknowledge financial support from Andalas University (LPPM) through the Doctoral Dissertation Research Recognition Grant (PDD) with contract number: 46/UN16.19/PT.01.03/PDD/2024.Author Contributions

Author Contributions

M.C. conducted the experiments, wrote the original draft, conceptualised, visualised, validated, used methodology, investigated, and analysed data. **S.H.** conducted the experiments, supervised the review, edited the manuscript, and developed the methodology. **R.T.** conducted the experiments, reviewed and edited them, supervised the process, and ultimately found a solution. **Y.** found a research idea, conducted the experiments, reviewed, edited, and supervised.

References

ANSI/AISC, & 341-16. (2016). *An American National Standard, Seismic Provisions for Structural Steel Buildings*. Chicago, American Institute of Steel Construction.

Azad, K. S., & Topkaya, C. (2017). A review of research on steel eccentrically braced frames. *Journal of Constructional Steel Research, 128*, 53-73. doi:10.1016/j.jcsr.2016.07.032

Binder, J., Gray, M., C, & O. (2017). Cast steel replaceable modular links for eccentrically braced frames. *Structures Congress*(University of Exeter). doi:10.1061/9780784480410.018

Bruneau, M., Uang, C., & Whittaker, A. (2011). *Ductile design of Steel Structures*. McGraw-Hill ISBN 978-0-07-162523-4.

Chacon, R., Vega, A., & Mirambell, E. (2019). Numerical study on stainless steel I-shaped links on eccentrically braced frames. *Journal of Constructional Steel Research, 159*, 67-80. doi:10.1016/j.jcsr.2019.04.014

Chairi, M., Zaidir, Haris, S., & Yurisman. (2023). Performance improvement of earthquake-resistant steel structure system EBF (Eccentrically Braced Frame) by using modified long links. *E3S Web of Conference 464*. Padang, Indonesia: EDP Sciences. doi:10.1051/e3sconf/202346402001

Daneshmand, A., & Hashemi, H. B. (2012). Performance of intermediate and long links in eccentrically braced frames. *Journal of Constructional Steel Research, 70*, 167-176. doi:10.1016/j.jcsr.2011.10.011

Dewi, S., Thamrin, R., Haris, S., & Yastari, F. (2024). Tensile Forces Behaviour on Longitudinal Reinforcement and CFRP Strips on Circular Hollow Reinforced Concrete Columns. *Civil and Environmental Engineering* , 86-97.

Dusicka, P., Itani, A. M., & Buckle, I. G. (2010). Cyclic Behavior of Shear Links of Various Grades of Plate Steel. *Journal of Structural Engineering, 136 (4)*, 370-378. doi:10.1061/(ASCE)ST.1943-541X.0000131

Engelhardt, M. D., & Popov, E. P. (1989). *Behaviour of long links in eccentrically braced frames*. UCB/EERC-89/0 1;University of California at Berkeley.

Engelhardt, M., & Popov, E. P. (1992). Experimental performance of long links in eccentrically braced frames. *Journal of Structural Engineering, 118*, 3067-3088. doi:10.1061/(ASCE)0733-9445(1992)118:11(3067)

Garmeh, V., Akbarpour, A., Adibramezani, M., Kashani, A. H., & Adibi, M. (2022). SMA-based self-centering eccentrically braced frame with vertical link member. *Structures, 43*, 1230-1258. doi:10.1016/j.istruc.2022.07.034

Ghobarah, A., & Ramadan, T. (1990). Seismic analysis of link of various length in eccentrically braced frames. *J. Civ. Eng, 18*, 140-148. doi:10.1139/l91-016

Gottem, A., Lingeshwaran, N., Kumar, Y., Chowdary, C., Pratheba, S., & Perumal, K. (2023). Analytical Study of Buckling Restrained Braced Frames in Different Seismic Zone Using ETABS. *Civil and Environmental Engineering, 19*(1), 426-443. doi:10.2478/cee-2023-0038

Hjelmstad, D., Keith, & Popov, E. P. (1984). Characteristics of eccentrically braced frames. *Journal of Structural Engineering, 110*, 340-353. doi:10.1061/(ASCE)0733-9445(1984)110:2(34

Kasai, K., & Popov, E. P. (1986). *A study of seismically resistant eccentrically braced frames.* UCB/EERC-86/01; University of California. Berkeley, California.

Kasai, K., & Popov, E. P. (1986). General behavior of WF steel shear link beams. *Journal of Structural Engineering, 112*, 362-382. doi:10.1061/(ASCE)0733-9445(1986)112:2(362)

Kurdi, Budiono, B., Moestopo, M., Kusumastuti, D., & Muslih, M. (2017). Residual stress effect on link element of eccentrically braced frame. *Journal of Constructional Steel Research, 128*, 397-404. doi:10.1016/j.jcsr.2016.09.006

Malley, O., James, & Popov, E. P. (1984). Shear links in eccentrically braced frames. *Journal of Structural Engineering, 110*, 2275-2295. doi:10.1061/(ASCE)0733-9445(1984)110:9(2275)

Mansouri, A. (2021). Development of a novel haunched link for eccentrically braced frames. *Engineering Structures, 245*, 112870. doi:10.1016/j.engstruct.2021.112870

Maulana, H., Thamrin, R., Kurniawan, R., Haris, S., Nabila, W. U., & Syaifa, L. (2025). Seismic Behaviour of Reinforced Concrete Beam-Column Joints Strengthened With Varied Installation Length of CFRP Sheets. *Civil and Environmental Engineering* , 409-426.

Mohebkhah, A. M. (2020). Shear resistance of retrofitted castellated link beams: Numerical and limit Analysis Approaches. *Engineering Structures, 203*, 109864. doi:10.1016/j.engstruct.2019.109864

Musbar, B. B., Kusumastuti, D., & Setio, H. D. (2017). Numerical study on the modification of long links in eccentrically braced frame. *AIP Conference Proceedings*. Bandung: American Institute of Physics. doi:10.1063/1.5011497

Rezaeian, A., Shayanfar, M., & Jelokhani, P. (2022). The Experimental Study of Eccentrically Braced Frames with Double Vertical Links. *Journal of Constructional Steel Research, 199*, 107587. doi:10.1016/j.jcsr.2022.107587

Roeder, C. W., & Popov, E. P. (1977). *Inelastic behaviour of eccentrically braced frames.* UCB/EERC-77/18;National Science Foundation, Washington, D.C.; American Iron and Steel Inst., Washington, D.C.

Roeder, C. W., & Popov, E. P. (1978). Cyclic shear yielding of wide-flange beams. *Journal of the Engineering Mechanics Division, 4*, 763-780. doi:10.1061/JMCEA3.0002378

SNI. (254 (2019)). *1726-2019 Earthquake Resistance Planning Procedures for Building and Non-Building Structures*. Jakarta.

Stephens, M., & Dusicka, P. (2014). Continuously stiffened composite web shear links: tests and numerical model validation. *Journal of Structural Engineering, 140*(7). doi:10.1061/(ASCE)ST.1943-541X.0000996

Yurisman, Army, B., Sari, D., & Chairi, M. (2021). Kajian Numerik Perilaku Seismik Link Geser Pada Sistem Struktur. *Jurnal Rekayasa Sipil, 17*, 204-217. doi:10.25077/jrs.17.3.204-217.2021

Yurisman, Budiono, B., Moestopo, M., & Suarjana, M. (2010). Behaviour of shear link of WF section with diagonal web stiffener of eccentrically braced frames (EBF) of steel structure. *Journal of Engineering and Technological Sciences,, 42*(2), 103-128. doi:10.5614/itbj.eng.sci.2010.42.2.1

Yurisman, Sari, D., Murdiansyah, L., Chairi, M., & Khadavi. (2025). Numerical Analysis of the Seismic Performance of Eccentrically Braced Frames (EBFs) in Earthquake Resistant Steel Structures with Modified Plate Stiffener Pattern in The Link Element. *Civil Engineering and Architecture, 13*(4), 2895-1913. doi:10.13189/cea.2025.130407

How to Cite This Article

Chairi, M., Haris, S., Thamrin, R., & Yurisman (2026). Seismic Behaviour of Long Links in Eccentrically Braced Frames Strengthened with Steel Plate and Diagonal Stiffener. Civil and Environmental Engineering, 0 (0). https://doi.org/10.2478/cee-2026-0076